# Symmetry in Strain Engineering of Nanomembranes: Making New Strained Materials

**Deborah M. Paskiewicz,[†] Shelley A. Scott,[†] Donald E. Savage,[†] George K. Celler,[‡] and Max G. Lagally[†,*]**

[†]University of Wisconsin, Madison, Wisconsin 53706, United States and [‡]Rutgers University, Piscataway, New Jersey 08854, United States

**ABSTRACT** Strain in a material changes the lattice constant and thereby creates a material with new properties relative to the unstrained, but chemically identical, material. The ability to alter the strain (its magnitude, direction, extent, periodicity, symmetry, and nature) allows tunability of these new properties. A recent development, crystalline nanomembranes, offers a powerful platform for using and tuning strain to create materials that have unique properties, not achievable in bulk materials or with conventional processes. Nanomembranes, because of their thinness, enable elastic strain sharing, a process that introduces large amounts of strain and unique strain distributions in single-crystal materials, without exposing the material to the formation of extended defects. We provide here prescriptions for making new strained materials using crystal symmetry as the driver: we calculate the strain distributions in flat nanomembranes for two-fold and four-fold elastically symmetric materials. We show that we can controllably tune the amount of strain and the asymmetry of the strain distribution in elastically isotropic and anisotropic materials uniformly over large areas. We perform the experimental demonstration with a trilayer Si(110)/$Si_{(1-x)}Ge_x$(110)/Si(110) nanomembrane: an elastically two-fold symmetric system in which we can transfer strain that is biaxially isotropic. We are thus able to make uniformly strained materials that cannot be made any other way.

**KEYWORDS:** nanomembranes · strain sharing · elastic relaxation · heterostructures · epitaxy · thin films

Strain modifies many important materials properties. In semiconductors, most salient features are affected by strain, including electronic band structure,[1−3] electronic transport,[4] optoelectronic properties,[5] phonon structure,[6] and kinetics and thermodynamics of atom motion and structure.[7] In oxides, the existence and extent of structural phases are sensitive to strain: magnetic, dielectric, and superconducting complex oxides can have extremely large responses to applied stresses and fields.[8] In thin-film technology, the stress state of the deposited film controls materials properties from optical reflectance to resistivity.[9,10] One would like to harness the strain to obtain unique properties not present in the relaxed material. Thermodynamics limits the success: the strain term in the free energy of a material quickly leads to the formation of extended defects,[11] which can limit expected new properties or enhanced performance.[12−14]

A recent development, crystalline nanomembranes (NMs), offers a new platform for creating strained materials that have unique properties. Crystalline NMs are extremely flexible, compliant, and very thin (less than 5−500 nm), with aspect ratios of thickness to lateral dimension on the order of $10^5$ or greater. These features allow introduction of strain in ways not possible with thick materials, enabling a panoply of entirely new properties. Use of NMs has already significantly altered the landscape as it relates to strain in semiconductors. For example, elastically strain-sharing NMs enable large-area, dislocation-free, uniformly strained silicon,[15,16] a development of considerable importance for enhancing charge carrier mobilities, for creating very-high-speed flexible electronics,[17,18] and for modifying band gaps and creating new types of electronic heterostructures and superlattices.[19−21] There is also potential for NM fabrication in other material systems, such as III−V semiconductors,[22] III-nitrides,[23] and various oxide materials,[24,25] all of which exhibit changes in materials properties with strain.[3,26−28] What has not been recognized, however, is that strain engineering of NMs offers the *opportunity to make uniformly strained materials that cannot be made any other way*, by taking advantage of the anisotropies in elastic constants of the components of the strained NM system.

We provide here a general treatment of elastic strain sharing in functional NM systems to demonstrate the influence of elastic anisotropies on the resulting strain distributions. Strain engineering of NMs can be accomplished using a multiple-layer functional structure fabricated on a release layer. This release layer is differentially etched to allow the functional structure to be free of a constraint during part of the process. If a layer of the functional NM structure

* Address correspondence to lagally@engr.wisc.edu.

Received for review March 14, 2011 and accepted June 18, 2011.

**Published online June 18, 2011**
10.1021/nn2009672

© 2011 American Chemical Society

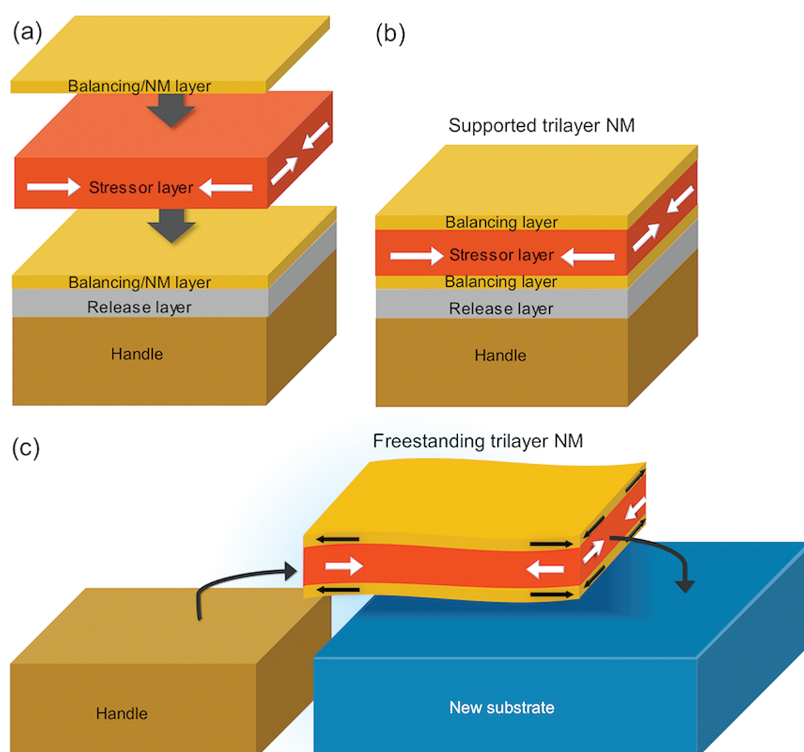


**Figure 1. Schematic diagrams of fabrication of elastically strain-sharing trilayer NM heterostructures. (a) Assembly of trilayer heterostructure: the stressor layer and top-balancing layer can be transferred *via* dry or wet lift-off techniques, epitaxially grown or non-epitaxially deposited. (b) Initial trilayer heterostructure constrained by a rigid attached substrate (after growth, deposition, or NM bonding). All of the strain is in the stressor layer. (c) Release and transfer of the free-standing trilayer heterostructure by removal of the release layer through selective etching processes. The arrows in the schematic diagram of the free-standing NM show the direction and approximate amount of strain in each of the layers. If the initial strain in the stressor layer is compressive (tensile), the strain transfer to the outer NM layers will be tensile (compressive). All of the layers are considered to be uniform in thickness, and the strain in the stressor layer is constant in the vertical direction.**

contains strain (the stressor layer), this strain is shared with the other layers once the system becomes free of the constraint of the substrate.[16]

To aid in understanding, we consider balanced trilayer NMs, in which the middle layer is initially strained and the initially unstrained top and bottom layers (balancing layers) are chemically and structurally (thickness and crystalline orientation) identical, so they become equally strained upon release and the NM remains flat during the elastic strain-sharing process (no curling occurs while it is unattached to any substrate).[29] A schematic diagram of the elastic strain-sharing process for balanced functional structures is shown in Figure 1.

The stressor layer can in principle be introduced by epitaxial growth, non-epitaxial growth, or membrane bonding. In each case, the strain in the middle layer originates from different sources: a lattice mismatch provides a fixed strain in the stressor layer for epitaxially grown films; there is a fixed amount of intrinsic strain in amorphous or polycrystalline films deposited *via* non-epitaxial growth techniques;[10] and in membrane bonding, the strain in the stressor layer can be introduced before bonding by controllable mechanical deformation[30] or differences in thermal expansion upon annealing.[31] Similarly, the balancing layers can be epitaxially grown, deposited, or transferred and bonded without strain. Because NMs are thin and ultracompliant, we can readily transfer and bond dissimilar materials.[32]

Once the stressor layer and balancing layers are joined to form one coherent functional heterostructure (Figure 1b), the entire trilayer NM is then freed from the substrate and allowed to strain share (Figure 1c): the free-standing trilayer heterostructure is allowed to reach mechanical equilibrium. A force balance model precisely predicts strain sharing between the layers. The novelty of elastically strain-shared NMs is that strain is *shared* between multiple layers during the free-standing stage, making it possible to engineer the amount of strain in each of the layers by varying relative thicknesses and compositions of the component layers.

## RESULTS AND DISCUSSION

When considering elastic strain sharing among several layers, considerations of the symmetry of the elastic constants of each layer and the initial mismatch strain distribution determine the detailed ultimate strain distribution in in-plane directions when the multilayer functional structure is released and the

strain is shared. In the only case so far investigated, based on (001)-oriented cubic material systems,[15,22] all layers of the structure have high (four-fold) crystalline symmetry. The elastic constants of (001)-oriented cubic materials are therefore also four-fold symmetric, and thus isotropic biaxial strain is expected when the mismatch strain between layers is equibiaxial, as is the case for epitaxially mismatched materials with similar crystalline structures.[31] In this case, a two-dimensional description (in-plane and out-of-plane) of the strain is sufficient to describe the strain in all layers.

When the elastic symmetry is lower, or when the symmetry of the different layers is mixed, one expects intriguing complexity in the strain distribution of individual layers. Here, we must use anisotropic linear elastic theory to properly describe the strain in each layer in three dimensions. The results lead to the ability to create unique strain distributions in thin sheets, something that in turn can lead to unique electronic, photonic,[27] and dielectric[33] properties.

The strain sharing in multilayer NM systems will depend on several factors, including relative thicknesses of each of the layers, differences in elastic properties of the materials, crystalline orientation, original mismatch strain distribution, twist angle of bonded layers, plastic deformation, and so on. To simplify this problem, we will consider only balanced systems, as described above, such that we can ignore any bending moment in the trilayer NM. The top and bottom layers are always identical in composition, orientation, and thickness. Effectively this can mean that the originally unstrained balancing layers are on the top and bottom (Figure 2a,b), or equal strained (stressor) layers are on top and bottom (Figure 2b,c). Assuming a balanced heterostructure mathematically reduces our trilayer problem to a bilayer problem, the force contributions from the top and bottom layers are equal and we only need to consider mismatch strain at one interface. The possible configurations are shown schematically in Figure 2. For the remainder of the paper, we will refer to trilayers as those shown in Figure 2a,b; however, all of the situations shown in Figure 2 are mathematically equivalent.

The force balance model used to determine the strain distributions in the free-standing trilayer NMs is based on two states: the initial state, in which the trilayer NM is attached to a handling substrate and the balancing layers contain no strain, and the final state, a free-standing trilayer NM that has been allowed to come to equilibrium. The initial, or as-grown, state of the trilayer assumes all of the strain is in the stressor or middle layer; this is the mismatch strain in the system. The mismatch strain distribution will depend on growth, deposition, or bonding conditions.

If we assume that all of the layers are coherent (no relaxation *via* slipping or extended-defect formation at interfaces), then the mismatch strain must stay constant

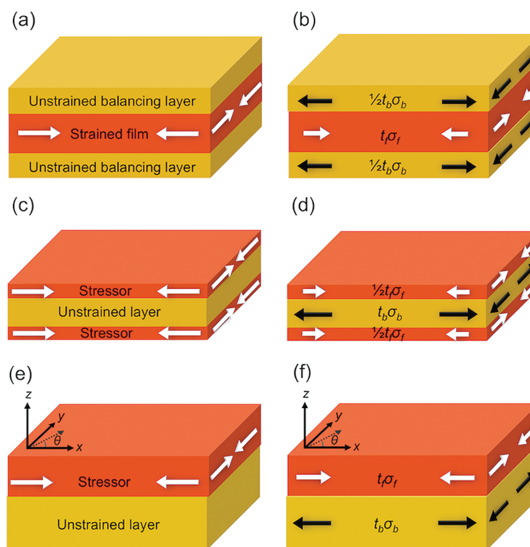


**Figure 2. Mathematically equivalent models of balanced trilayer NMs. The arrows represent the relative magnitude and direction of the strain in each layer. The initially unstrained layers can be on the top and bottom (a), or the initially unstrained layer can be sandwiched between two stressor layers (c). Both of these cases are mathematically equivalent to a bilayer system in which the two outer-layer thicknesses are added and represented as one layer (e). The figures on the left (a,c,e) show the initial state of each system: all of the strain remains in the stressor layer while attached to the initial handling substrate. The figures on the right (b,d,f) show the final state of the heterostructures after the NM has been allowed to strain share. The coordinate system is defined in the same way for all layers; however, the crystallographic directions in the stressor and initially unstrained layer need not be aligned.**

throughout the strain-sharing process; that is, the difference between the strain in the stressor layer ($\varepsilon_f$) and the strain in the outer balancing layers ($\varepsilon_b$) must be equal to the mismatch strain ($\varepsilon_m$)

$$\varepsilon_m = \varepsilon_f - \varepsilon_b \tag{1}$$

where each strain term can be written in tensor form[31] as

$$\varepsilon_i = \begin{pmatrix} \varepsilon_{xx} & \varepsilon_{xy} & \varepsilon_{xz} \\ \varepsilon_{xy} & \varepsilon_{yy} & \varepsilon_{yz} \\ \varepsilon_{xz} & \varepsilon_{yz} & \varepsilon_{zz} \end{pmatrix} \tag{2}$$

We use tensor quantities here to describe fully the strain in each of the layers of our trilayer NM system, such that we can use any mismatch strain distribution; we are not restricted to assuming an equibiaxial mismatch strain distribution. Once the trilayer structure is allowed to share the strain elastically, the free-standing NM will equilibrate (Figure 1c); compressive (tensile) strain in the stressor layer will transfer as tensile (compressive) strain to the outer balancing layers. The total force in the top and bottom layers must be equal and opposite to the force in the middle layer; the sum of the forces in the trilayer NM structure should equal zero:

$$C_f\varepsilon_f t_f + C_b\varepsilon_b t_b = 0 \tag{3}$$

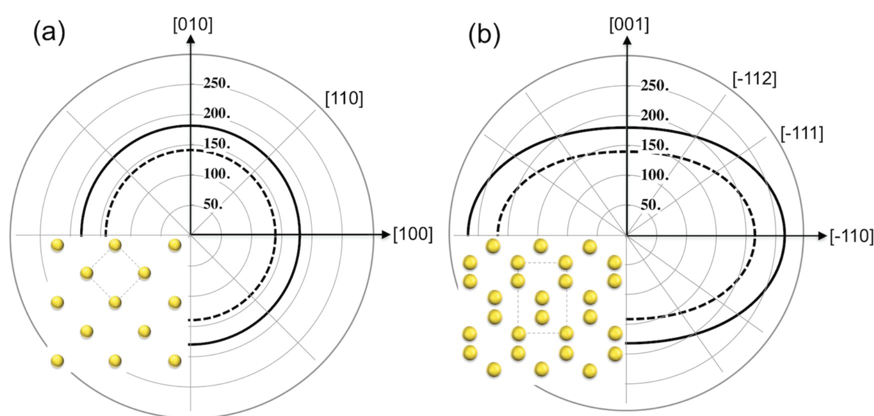


**Figure 3. Biaxial modulus, *M*, for Si (—) and Ge (- - -) as a function of in-plane direction on the (a) (001) surface and (b) (110) surface. The insets in each graph show the atomic arrangement in the (001) and (110) planes, respectively. The crystallographic and elastic symmetry is four-fold for the (001) surface orientation and two-fold for the (110) surface orientation.**

The force in each layer is taken to be the stress, $\sigma_i = C_i\varepsilon_i$, multiplied by the thickness ($t_i$) of each layer,[31] where $C_i$ is the fourth-rank stiffness tensor and $\varepsilon_i$ is the strain tensor for the respective layer (see Materials and Methods section for details). We are assuming that there is negligible thickness variation of the layer such that $t_i$ is a constant scalar quantity. An expression for the strain in the balancing layers is obtained by combining eqs 1 and 3 and dividing through by the stressor-layer thickness ($t_f$):

$$C_f\varepsilon_m + C_f\varepsilon_b + \eta C_b\varepsilon_b = 0 \quad (4)$$

where $\eta$ is defined as the thickness ratio between the balancing layers and the strained film (or stressor layer), $t_b/t_f$.

It is apparent from eq 4 that the strain transferred to the outer balancing layers when the trilayer NM is released from the handling substrate will depend on the symmetry of the initial strain distribution in the stressor layer ($\varepsilon_m$), the relative stiffness differences between the balancing layers and the stressor layer ($C_b$ and $C_f$, respectively), and the ratio of thicknesses of each of the layers ($\eta$). We consider four situations. We (1) start with the outer balancing layers and the stressor layer both having four-fold elastic symmetry with equibiaxial mismatch strain ($\varepsilon_{xx} = \varepsilon_{yy} = \varepsilon_m$), (2) change the elastic symmetry of the entire system while maintaining an equibiaxial mismatch strain, and then (3,4) consider mixed-elastic-symmetry systems with equibiaxial strain and anisotropic biaxial strain ($\varepsilon_{xx} \neq \varepsilon_{yy} \neq 0$), respectively.

The goal of this work is to investigate the changes in the transferred-strain distribution as a function of in-plane direction in free-standing trilayer NMs based on differences in elastic symmetry of the materials in the heterostructure. For simplicity, we limit ourselves to materials with four-fold elastic symmetry (biaxially isotropic) and materials with two-fold elastic symmetry (biaxially anisotropic), but eq 4 can be used on any balanced trilayer NM system if the crystalline orientation of the materials, elastic constants, and mismatch strain distribution are known.

To illustrate the difference between four-fold and two-fold elastic symmetry, Figure 3 shows the biaxial modulus, *M*, as a function of in-plane direction for (001)- and (110)-oriented Si and Ge. The biaxial modulus is $M = E/(1 - \nu)$, where *E* is the elastic (Young's) modulus and $\nu$ is Poisson's ratio; both are a function of crystallographic orientation.[34] The plots of the biaxial modulus as a function of in-plane orientation illustrate how the material will respond to an equibiaxial stress in that plane: a constant biaxial modulus (Figure 3a) means that for an applied equibiaxial stress an equibiaxial strain results. The biaxial modulus for the two-fold elastically symmetric material (Figure 3b) is not constant, and therefore, some anisotropic biaxial strain will result for a similar stress. The insets in Figure 3a,b show the crystalline symmetry of the (001)- and (110)-oriented diamond cubic materials, respectively. The crystalline symmetry of the material matches the elastic symmetry.

Case 1: First we consider the case where all of layers in the trilayer heterostructure are biaxially elastically isotropic and the mismatch strain is equibiaxial. We use a (001)-oriented trilayer heterostructure system with an epitaxial mismatch strain as an example.[15] An isotropic biaxial mismatch strain would also result from a deposited amorphous or polycrystalline stressor layer (with an inherent stress from deposition) that has isotropic elastic symmetry. Figure 4a shows the normal in-plane strain distribution in the balancing layers upon elastic strain sharing with a stressor layer with an initial mismatch strain of ~0.8% (red) for various thickness ratios, $\eta$. Here, the normal in-plane strains of the balancing layer are equal ($\varepsilon_{xx} = \varepsilon_{yy}$) and there is no shear strain ($\varepsilon_{xy} = 0$). Recall that the mismatch strain is the original strain in the stressor layer before release of the trilayer NM, but that the sign of the strain transferred to the outer balancing layers is opposite to the original strain in the stressor layer. Notice that as

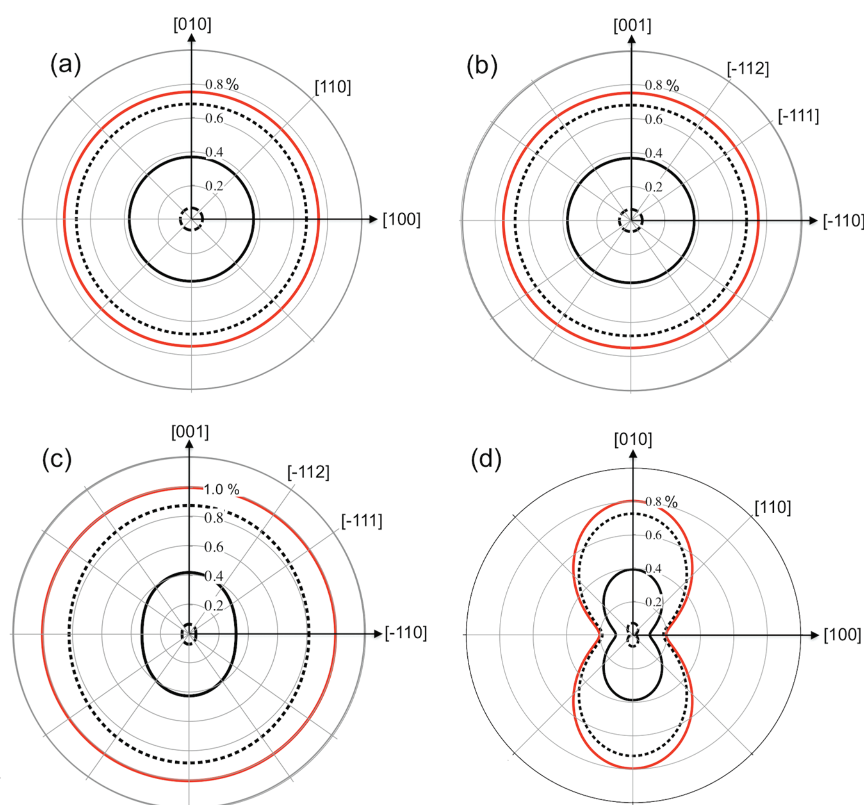


**Figure 4. In-plane strain distributions in the balancing layers of trilayer NMs after elastic strain sharing for: (a) case 1, biaxially isotropic balancing layers with a biaxially isotropic stressor layer; (b) case 2, biaxially anisotropic balancing layers with a biaxially anisotropic stressor layer; (c) case 3, biaxially anisotropic balancing layers with an isotropic stressor layer; (d) case 4, biaxially isotropic balancing layers with a biaxially anisotropic stressor layer. Each curve represents a different thickness ratio, $\eta = t_b/t_f$: $\eta = 0.1$ (···), $\eta = 1.0$ (—), and $\eta = 10$ (- - -). The mismatch strain in the system is also shown (red solid line); this corresponds to the strain in the stressor layer before strain sharing occurs and is of opposite sign as the strain transferred to the outer balancing layers. The radial distance to any curve is the magnitude of the strain in that direction. The elastic constants for Si are used for the balancing layers, and the elastic constants of the stressor layer vary with each case (see Materials and Methods section for details).**

the stressor layer gets thicker and the balancing layers thinner ($\eta$ decreases), more strain is transferred to the balancing layers. Larger strain transfer is also possible with increased mismatch strain.

Case 2: As a next limit, we consider a heterostructure system in which all of the layers have two-fold elastic symmetry but with an equibiaxial mismatch strain distribution. An example of this type of heterostructure is coherent epitaxial growth and release of a (110)-oriented trilayer heterostructure.[35,36] The mismatch strain is isotropic in-plane because we are using balancing layers and stressor layers with similar crystalline structures where the same in-plane orientations align during epitaxial growth [*e.g.*, SiGe(110) on Si(110)]. This means that the mismatch strain is defined in a similar way as a trilayer grown on (001)-oriented cubic materials (see Materials and Methods section for details). Recall, for example, from Figure 3 that the biaxial modulus of Si(110) is biaxially anisotropic; however, the similar crystal structures of Si and Ge result in similar elastic-constant anisotropies. The implication is that strain transfer between (110)-oriented materials of similar crystalline structures remains biaxially isotropic (Figure 4b). *We believe there is no other way to make such strain distributions.*[37−39] These biaxially isotropic strain distributions are only enabled by elastic strain engineering in NMs.

Case 3: The third situation for elastic strain sharing is that of an elastically isotropic stressor layer between layers of elastically two-fold symmetric balancing layers. An example is a deposited amorphous thin film between two (110)-oriented cubic single-crystalline NMs. Here we assume an equibiaxial mismatch strain (see Materials and Methods section for details), and that the strain is constant through the thickness of the elastically isotropic strained film. These are reasonable assumptions for a truly randomly oriented polycrystalline or amorphous intrinsically strained metal thin film: the elastic properties of the film are isotropic, and the force exerted by the film varies linearly with film thickness.[40] Recall that the mismatch strain remains constant for coherent films for any given strain-sharing condition (eq 1). In this case, coherency of the layers means that the atoms at the interface between the two materials do not slip or rearrange during strain sharing: the bonding points at the interfaces between the

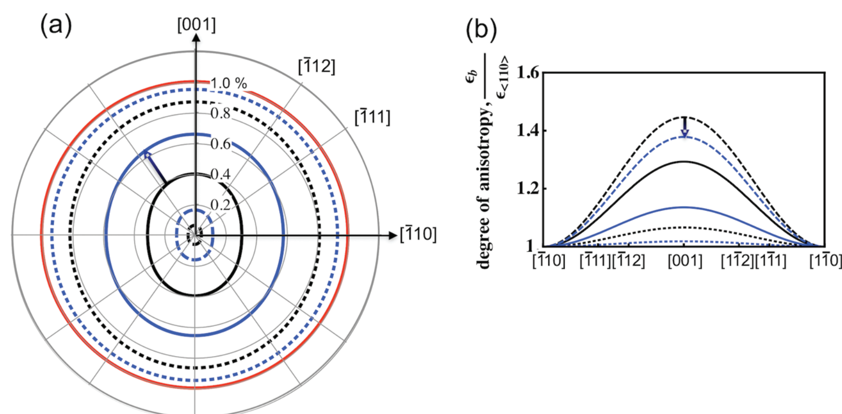


**Figure 5. (a) Strain transferred to outer balancing layers for a heterostructure like case 3: two-fold elastically symmetric balancing layers with four-fold elastically symmetric stressor layer. The mismatch strain is equibiaxial (red solid line). The transferred strain is shown for three different thickness ratios: $\eta$ = 0.1 (···), $\eta$ = 1.0 (—), and $\eta$ = 10 (- - -) and and two stiffnesses of the stressor layers (black curves and blue curves). The stressor layer elastic modulus is slightly smaller than that of the balancing layers for the black curves and is larger by about a factor of 3 for the blue curves. The radial distance to any curve is the magnitude of the strain in that direction. The arrow indicates the increase in magnitude of the transferred strain for an increase in stressor layer elastic modulus for the same thickness ratio (example shown for $\eta$ = 1.0). (b) Degree of anisotropy is taken to be the magnitude of the strain in a given direction normalized by the strain in the ⟨110⟩-type direction. The curve line types in (b) correspond to the same situations as the curves in (a). The magnitude of strain transfer is larger for stressor layers with larger elastic moduli, but the degree of anisotropy decreases (as shown by arrow for $\eta$ = 0.1 curves).**

stressor layer and balancing layers do not change. Because the mismatch strain is equibiaxial, any anisotropy in the strain distribution in the two-fold elastically symmetric balancing layers after elastic strain sharing is a direct result of the elastic anisotropy of the balancing layers. We assume an in-plane mismatch strain of $\varepsilon_o$ = 1% and choose elastic constants for the stressor layer that are similar in stiffness to the balancing layers (but isotropic) (see Materials and Methods section for details). The resulting strain distribution in the low-elastic-symmetry balancing layers after elastic strain sharing is shown in Figure 4c. The strain distribution in the low-elastic-symmetry balancing layers has varying degrees of anisotropy as a function of thickness ratio, $\eta$. The degree of anisotropy in the strain distribution is discussed below and shown in Figure 5b.

Case 4: Finally, the fourth situation is a uniaxially mismatched system in which the stressor layer has two-fold elastic symmetry and the outer balancing layers are elastically isotropic in-plane [*e.g.*, (001)-oriented cubic single-crystalline NM]. A uniaxially mismatched system is one in which the lattice mismatch is large in one in-plane direction and smaller perpendicular to that: the mismatch strain is now a function of in-plane direction. The strain can be introduced *via* growth or *via* bonding a prestrained membrane between two unstrained ones, something that is feasible because membranes bond very well. A strain mismatch of this sort occurs for a hexagonal material growing in a [1$\bar{1}$00] orientation on a (001)-oriented cubic surface[41] or by bonding a mechanically anisotropically deformed stressor layer between elastically biaxially isotropic balancing layers. For simplicity, we assume a mismatch strain in which the normal in-plane strains are $\varepsilon_{xx} = \varepsilon_m$, $\varepsilon_{yy} = a\varepsilon_m$, and $\varepsilon_{xy} = 0$. Where the *x*-direction in the film {[$\bar{1}$10] on a (110)-oriented surface} is aligned with the [110] direction on the cubic (001) surface. This scenario is reasonable either for well-aligned NM transfer[42] or for epitaxial growth with a uniaxial mismatch, in which the direction of highest mismatch is aligned in only one of the ⟨110⟩-type directions (*i.e.*, no twins); a situation that can occur if the hexagonal film is grown on a patterned or vicinal (001)-oriented cubic surface.[43] In our description, the elastic constants for the stressor are arbitrarily chosen such that the soft direction (low elastic modulus) of the stressor layer is aligned in the direction of highest mismatch strain. The strain distribution in the balancing layers after strain sharing is shown in Figure 4d, assuming a $\varepsilon_m$ = 0.2% and $a$ = 4. The strain transferred to the balancing layers follows the symmetry of the mismatch strain closely. That is, we can take a four-fold crystallographically symmetric surface orientation and apply strain to create a material with two-fold crystallographic symmetry. Lattice deformation of this sort is equivalent to applying a small in-plane isotropic biaxial strain and a uniaxial strain at the same time. The ability to break the symmetry in highly crystallographically symmetric materials offers opportunities to exploit new materials properties not seen otherwise, such as demonstration of the linear electro-optic effect in Si[44] and antiferromagntism in certain dielectric oxides.[45]

We have shown that the strain distributions in elastically strain-shared NMs depend on the elastic symmetry of the two materials and the initial mismatch strain distribution between the layers of a functional

trilayer NM. Additionally, the magnitude of strain transferred to the outer balancing layers can be tuned by varying the thickness ratio ($\eta$). We show in Figure 4 that as we increase the thickness of the stressor layer with respect to the balancing layers (decrease $\eta$) that more strain is transferred to the balancing layers.

It is important to note that the above strain-sharing analysis is only valid for *elastically* deformed layers. In order to avoid plastic relaxation of any of the layers during strain sharing, the absolute thickness of each of the layers is just as important as the relative thickness ratio. As the layers get thicker (more bulk-like), less elastic strain is accommodated by the material before plastic deformation occurs. The strain energy is proportional to thickness, and at some point, it will become energetically favorable for the material to deform plastically to relieve strain[31] rather than share strain elastically. The thinness of NMs enables elastic strain sharing. If the dimensions of all of layers were scaled to the wafer level (*e.g.*, similar trilayers made with wafer bonding), delamination and fracture would occur for similar strain levels.

Even at the nanometer scale, the thicknesses of the layers in the NM system need to be kept below the critical thickness for plastic relaxation at all stages of the NM fabrication process.[11,46] Keeping layers below this critical thickness ensures that we can introduce strain into materials without introducing defects. This capability is of considerable importance when considering integration of epitaxially or thermally mismatched materials for high-performance applications where strain is desired, but where the presence of any materials defects will significantly decrease device performance. Examples include group IV strained quantum wells for quantum computing devices,[47] strained superlattices for group IV quantum cascade lasers,[14] and group III−N growth for solar-cell applications.[48] In such materials applications, strain profiles are currently controlled by defect generation,[49] such that the magnitude and direction of strain cannot be engineered for optimum materials properties.

While the thinness of NMs allows us to introduce large amounts of strain without defects, the transferability of NMs allows us to incorporate materials with differing elastic constants to give another parameter to tune the strain transfer we see in trilayer NM systems. We have already demonstrated how varying the elastic symmetry of individual layers affects the transferred-strain distributions. For clarity in Figure 4, we used stressor layers with elastic constants of similar magnitudes to those of the balancing layers to highlight the effects of varying thickness ratios and elastic symmetry.

Because we can create trilayer NM systems by transfer processes, we can incorporate materials with different stiffnesses to enhance strain transfer. By using stressor materials that are "stiffer" (higher modulus) with balancing layers that are "softer" (lower modulus), there is less resistance on the stressor layer such that it can relax more completely, thus transferring higher amounts of strain to the softer balancing layers. The effect of controlling the stiffness of layers is shown in Figure 5 for the trilayer systems described in case 3. The second set of curves (blue) in both plots represents the same thickness ratio as the original curves (black), but the stiffness of the strained layer is increased by a factor of ~3. The strain transferred to the balancing layers increases with increasing stressor layer elastic modulus (Figure 5a), but the degree of anisotropy for this particular case (case 3: two-fold elastically symmetric balancing layers with elastically isotropic stressor layer) decreases (Figure 5b). Here we define the degree of anisotropy as the ratio of strain values in the balancing layers in orthogonal directions in-plane ($\varepsilon_{\langle 001\rangle}/\varepsilon_{\langle 110\rangle}$). As the thickness ratio increases (thickness of balancing layers increases, thickness of stressor layer decreases), the degree of anisotropy increases, but less strain is transferred to the balancing layers.

The change in degree of anisotropy is a result of the average elastic properties of the system. When the elastic moduli are similar (black curves in Figure 5), the average elastic properties are scaled by the thickness ratio of the materials: thicker balancing layers means more anisotropic-like elastic properties but also less strain transfer upon strain sharing. If the elastic modulus of the stressor layer is increased (blue curves in Figure 5), then the average elastic properties of the system are also scaled by the effective stiffness differences between the materials. For the same thickness ratio, the overall system with the stiffer stressor will act more isotropic-like because the materials properties of the stressor dominate the system. This is an important consideration when combining dissimilar materials: semiconductors on polymers for flexible electronics[18] or dielectric oxides on semiconductors for nanoelectronics.[50]

Thus far we have limited ourselves to trilayer systems in which the top and bottom layers are identical in chemical composition, crystalline orientation, and mechanical properties, such that we can mathematically consider a bilayer system with one interface. This elastic strain-sharing analysis can be extended to $n$-layer systems as long as the mismatch strain distribution at each interface and the elastic properties of each of the layers are known. For an $n$-layer system, there will be $n-1$ coherency equations (one for each interface similar to eq 1). Assuming a balanced system, a free-standing NM heterostructure will remain flat and the forces in the heterostructure will still be in equilibrium. This condition produces an equation similar to eq 3 with a term ($t_iC_i\varepsilon_i$) for each layer. To ensure that the $n$-layer system is balanced and will exhibit strain sharing without curling, the forces through the thickness of the structure must be equal and opposite. One way to ensure this is to calculate the radius of curvature for the heterostructure in the free-standing state,[31] if the radius is very

large compared to the lateral size of the NM, or infinite, the structure will remain flat during strain sharing and the above analysis is valid. This type of analysis would be needed to calculate strain sharing in complex superlattice systems or if using dissimilar materials for balancing layers (top and bottom layers not identical).

Equation 4 provides, in a compact form, a powerful description of how one can tune strain in a thin sheet by taking advantage of the elastic anisotropy in the thin sheet and controlling the stress and elastic anisotropy in the stressor layer. As alluded to earlier, we can introduce stress in the stressor layer by NM bonding, by heteroepitaxial growth, or by polycrystalline or amorphous-film deposition.

We provide here an experimental proof of case 2: heteroepitaxial growth of a stressor layer and outer balancing layer both with two-fold structural and elastic symmetry, but resulting in isotropic in-plane strain, namely, epitaxial growth and release of a Si(110)/$Si_{(1-x)}Ge_x$(110)/Si(110) trilayer NM. In this case, the SiGe(110) and top Si(110) layers are pseudomorphically grown on the template layer of (110)-oriented silicon-on-insulator (SOI). The thin Si(110) template layer of the SOI serves as the bottom balancing layer and is separated from the thick Si handle wafer by a buried oxide (BOX) release layer. The SiGe stressor layer is initially compressively strained because Ge has a larger lattice constant than does Si. Once the BOX layer is removed by selective etching, the trilayer Si/SiGe/Si(110) functional NM is allowed to strain share and some of the compressive strain from the SiGe layer is transferred as tensile strain to the outer Si layers.

We measured the in-plane lattice constants in two dissimilar perpendicular in-plane directions with X-ray diffraction to confirm that the strain sharing in these structures is indeed biaxially isotropic. Furthermore, we can tune the amount of *isotropic* in-plane strain in the Si balancing layers of a trilayer Si(110) NM up to ~0.7%[36] by changing the Ge composition (alters the mismatch strain, $\varepsilon_m$) of the alloy layer or the layer thickness ratio ($\eta$). This result is in distinct contrast to the anisotropic strain produced in Si epitaxially grown on conventional relaxed bulk SiGe(110) substrates: anisotropic strain relaxation of the SiGe(110) alloy results in anisotropic strain in the Si grown on top.[38]

## CONCLUSIONS

The above experiment is just one of many possible demonstrations of the power of nanomembrane technology to create strain distributions in materials not possible in any other way. Strain is in essence the ability to tune the lattice constant of a material, and elastic strain sharing in NMs offers a unique way to deform single-crystal materials in sheet form in order to harness potential advantages from strain without the introduction of crystalline defects.

We have effectively taken what would conventionally be considered the "substrate" (balancing layers) material and thinned it down to be of similar thickness as that of the "film" (stressor layer). In this way, we can introduce significant strain in a thin sheet of a material where the conventional bulk form of the material will contain effectively no strain for a similar thickness stressor layer. With the freedom of materials integration that NMs offer, we can incorporate strain distributions not easily achieved with other methods into materials with proper elastic strain engineering.

Our calculations show that by combining materials with two-fold and four-fold elastic symmetry one can produce anisotropic biaxial strain distributions in biaxially isotropic materials and isotropic biaxial strain distributions in biaxially anisotropic elastic materials. We have shown, as an example, experimental evidence in one such system: introducing isotropic biaxial tensile strain in a two-fold crystallographically symmetric material system, epitaxially grown Si/$Si_{(1-x)}Ge_x$/Si(110) NM heterostructures. By using knowledge of the elastic anisotropy of the crystalline stressor layer and the outer Si layers, we are able to induce and measure isotropic biaxial strain in Si(110). We have also been able so far to tune the strain in the trilayer Si(110) NMs controllably up to ~0.7% without the introduction of crystalline defects for strain relaxation. A consequence of elastic strain sharing in NMs is virtually defect-free material, which could enable materials engineering for high-performance applications where materials properties are sensitive to strain, but superior material quality is required. The calculations and fabrication methods described here are general and can easily be extended to other materials systems with minor modifications.

## MATERIALS AND METHODS

**Calculation Parameters.** To solve for each of the components of the balancing layer strain tensor ($\varepsilon_b$ in eq 4 in the text), we used the reduced form of the stiffness tensor and strain tensors. In general, the fourth-rank stiffness tensor can be mathematically reduced to a 6 × 6 matrix based symmetry on elastic constants.[51] At most, there will be 21 unique elastic constants ($C_i$ is a symmetric matrix). Here, we only consider cubic materials such that there are only three unique elastic constants and the stiffness tensor can be reduced to the following 6 × 6 matrix for NMs in which the Cartesian coordinate system is oriented along ⟨100⟩-type crystalline directions:

$$C_i = \begin{pmatrix} c_{11} & c_{12} & c_{12} & 0 & 0 & 0 \\ c_{12} & c_{11} & c_{12} & 0 & 0 & 0 \\ c_{12} & c_{12} & c_{11} & 0 & 0 & 0 \\ 0 & 0 & 0 & c_{44} & 0 & 0 \\ 0 & 0 & 0 & 0 & c_{44} & 0 \\ 0 & 0 & 0 & 0 & 0 & c_{44} \end{pmatrix} \quad (5)$$

where $c_{ij}$ are the elastic constants for the respective layer.[31] For systems in which the ⟨100⟩-type crystalline directions do

ARTICLE

**TABLE 1. Elastic Constants for the Various Materials Used for the Strain-Sharing Calculation in This Paper (All Units Are GPa)**

| material | layer | $c_{11}$ | $c_{12}$ | $c_{44}$ |
|---|---|---|---|---|
| Si[a] | balancing | 166.2 | 64.4 | 79.8 |
| $Si_{(1-x)}Ge_x$[b] | stressor | $166.2 - 37.8x$ | $64.4 - 16.2x$ | $79.8 - 13.1x$ |
| a-Si[c,e] | stressor | 131 | 64 | 37 |
| a-Ge[c,e] | stressor | 110 | 43 | 34 |
| a-Cr[d,e] | stressor | 314.1 | 83.4 | 115.3 |

[a] Si was used as the balancing layers in all plots.[31] [b] Linear combination of Si and Ge elastic constants based on alloy concentration. This is valid based on ref 52. $Si_{0.80}Ge_{0.20}$ was used as the stressor layer in Figure 4a,b,d. [c] Amorphous Si[53] was used as the stressor layer in Figure 4c, and a-Ge was used as the "softer" stressor layer in Figure 5a. [d] Amorphous Cr elastic constants are calculated values assuming an isotropic material based on elastic modulus and Poisson's ratio.[31] a-Cr was used as the "stiffer" stressor layer in Figure 5a. [e] For ideal isotropic materials, there are only two unique elastic constants: $c_{44} = 1/2(c_{11} - c_{12})$.

not align on the *xyz* Cartesian coordinate system (*z*-direction always oriented along surface normal), the stiffness matrix was transformed to reflect the new, rotated coordinate system,[51] such as was the case for (110)-oriented crystalline materials. Table 1 gives a list of elastic constants for the materials used as balancing layers and stressor layers in this paper. The Si−Ge system was used as an example, but the elastic constants of other crystalline materials could easily be substituted for these values. On the basis of similar symmetry arguments, the second-rank strain tensor can be reduced to

$$\varepsilon_i = \begin{bmatrix} \varepsilon_{xx} \\ \varepsilon_{yy} \\ \varepsilon_{zz} \\ 2\varepsilon_{xz} \\ 2\varepsilon_{yz} \\ 2\varepsilon_{xy} \end{bmatrix} \quad (6)$$

If we use the reduced matrix forms of the strain tensors and stiffness tensors, eq 4 is effectively a system of six equations and six unknowns (one for each of the components of the balancing layer strain tensor). Table 2 shows the components of the mismatch strain tensor for each of the cases considered. The plots in Figure 4 of the text show the in-plane normal strains ($\varepsilon_{xx}$ and $\varepsilon_{yy}$) as a function of in-plane direction after strain sharing.

**$Si/Si_{(1-x)}Ge_x/Si(110)$ NM Fabrication.** To create the functional strained NMs described above, we start with SOI(110), which consists of a thin Si(110) template layer (balancing layer) bonded *via* $SiO_2$ (release layer) to a Si(001) handle wafer. The starting template layer thickness is ~70 nm and is reduced to optimum thicknesses (usually ~10 nm) with thermal oxidation. We use solid-source molecular beam epitaxy (MBE) to grow the $Si_{(1-x)}Ge_x$ and top Si layers on SOI(110). MBE allows us to grow the heterostructures at a low temperature (450 °C) while independently controlling the growth rates (0.3−0.5 Å/s). The low-temperature bound is set by the need to maintain an approximately constant temperature with resistive heating. The clean surface was monitored with reflection high-energy electron diffraction (RHEED). After growth, etchant access holes are patterned with photolithography and reactive ion plasma etching. The NMs are subsequently placed in 49% hydrofluoric acid (HF) to etch away the underlying $SiO_2$ layer to create a free-standing Si(110) trilayer NM. The etch time depends on the etch hole size and spacing. During the release process, this trilayer NM is free of substrate constraints and can thus share strain elastically: the compressively strained $Si_{(1-x)}Ge_x$ middle layer partially relaxes (expands), transferring tensile strain to the sandwiching Si layers. The temporarily free Si(110) trilayer NM can either settle onto the handling substrate or can be floated

**TABLE 2. Components of the Mismatch Strain Tensor for Each of the Cases Considered**

| | $\varepsilon_{xx}$ | $\varepsilon_{yy}$ | $\varepsilon_{zz}$ |
|---|---|---|---|
| case 1[a] | $\varepsilon_m$ | $\varepsilon_m$ | $-(2c_{12}/c_{11})\varepsilon_m$ |
| case 2[a] | $\varepsilon_m$ | $\varepsilon_m$ | $-(c_{11}+3c_{12}-2c_{44})/(c_{11}+c_{12}+2c_{44})\varepsilon_m$ |
| case 3[b] | $\varepsilon_m$ | $\varepsilon_m$ | $-(2c_{12}/c_{11})\varepsilon_m$ |
| case 4[c] | $\varepsilon_m$ | $a\varepsilon_m$ | $-(c_{11}+3c_{12}-2c_{44}-2ac_{12})/(c_{11}+c_{12}+2c_{44})\varepsilon_m$ |

[a] $\varepsilon_m$ = mismatch strain between Si and $Si_{0.8}Ge_{0.2}$. [b] $\varepsilon_m = 1.0\%$. [c] $\varepsilon_m = 0.2\%$, $a = 4$.

free in water and can thus be easily transferred to a variety of other substrates.

**Strain Characterization.** Throughout the fabrication process, the Si(110) NMs are characterized with X-ray diffraction (XRD) to measure alloy composition, ensure proper strain states, and measure strain transfer in the released Si(110) NMs. High-resolution $\theta/2\theta$ triple-axis line scans around the (220) reflection allow us to characterize layer thicknesses, Ge composition, and the out-of-plane strain change, while off-axis reciprocal-space maps (RSMs) taken around the (331) and (260) reflection measure in-plane lattice constants in the [001] and [$\bar{1}$10] directions, respectively (Figure 6a,b). With accurate simulations of the line scans through the (220) reflections of the as-grown structures, we can confirm that the expected strain, as calculated with eq 4 in the text, matches the measured in-plane strain transfer. Figure 6c shows an example of $\theta/2\theta$ (220) line scans before and after release [a $\theta/2\theta$ scan around the (004) reflection of the Si(001) bulk substrate is used as reference]. The main peak, from the SiGe layer, shows a shift to a higher Bragg angle, indicating a reduction in the out-of-plane lattice constant. From this measurement, we can say that the SiGe layer becomes less compressively strained, transferring some of the compressive strain as tensile strain in the top and bottom Si layers. We determine the amount of in-plane strain in the Si layers by relating the out-of-plane strain change in the alloy layer during release to the in-plane strain change. If the strain transfer is truly elastic, the strain change in the alloy layer will equal the amount of tensile strain in the Si layers. The out-of-plane strain, $\varepsilon_\perp$, obtained from the (220) line scans, can be related to the in-plane strain, $\varepsilon_\parallel$, with eq 7

$$\varepsilon_\parallel = \frac{c_{11} + c_{12} + 2c_{44}}{c_{11} + 3c_{12} - 2c_{44}}\varepsilon_\perp \quad (7)$$

Here $c_{ij}$ are the elastic constants from the elastic stiffness tensor for SiGe (see Table 1). The presence of thickness fringes before and after release, as well as the uniform shift of all of the peaks, indicates that the layers remain coherent through strain sharing and that the strain sharing is elastic.

The RSMs around the (331) and (260) reflections (shown in Figure 6a,b) were used to confirm that the strain sharing in the Si(110) trilayer NMs is indeed biaxially isotropic. These reflections allowed us to measure the in-plane lattice constants in the [001] and [$\bar{1}$10] in-plane directions, respectively. We created a trilayer Si(110) NM in which some of the membrane was allowed to strain share, while a portion was still attached to $SiO_2$. The latter provides a reference of the intact as-grown structure. In both reflections, there is little in-plane peak broadening and all of the peaks align along the direction normal to the film surface, indicating that the in-plane lattice constant remains the same throughout the thickness of the film; that is, the SiGe in-plane lattice constants match those of the Si layers. Any relaxation of the alloy layer would be indicated by a broadening and in-plane shift of the SiGe peak toward the relaxed SiGe line. From Figure 6a,b, we can see that the membranes remain fully coherent (*i.e.*, an epitaxial relationship without interface dislocations is maintained) after the strain-sharing process, as well. If the strain in the Si layers were not a result of the strain sharing with the alloy layer, the in-plane lattice constants of the Si and SiGe would not match; two main peaks would be visible for both the released and as-grown portions of the RSMs, indicating one horizontal position for the Si layers and another position for the SiGe layer. The absence of a Si peak in the RSMs shown in

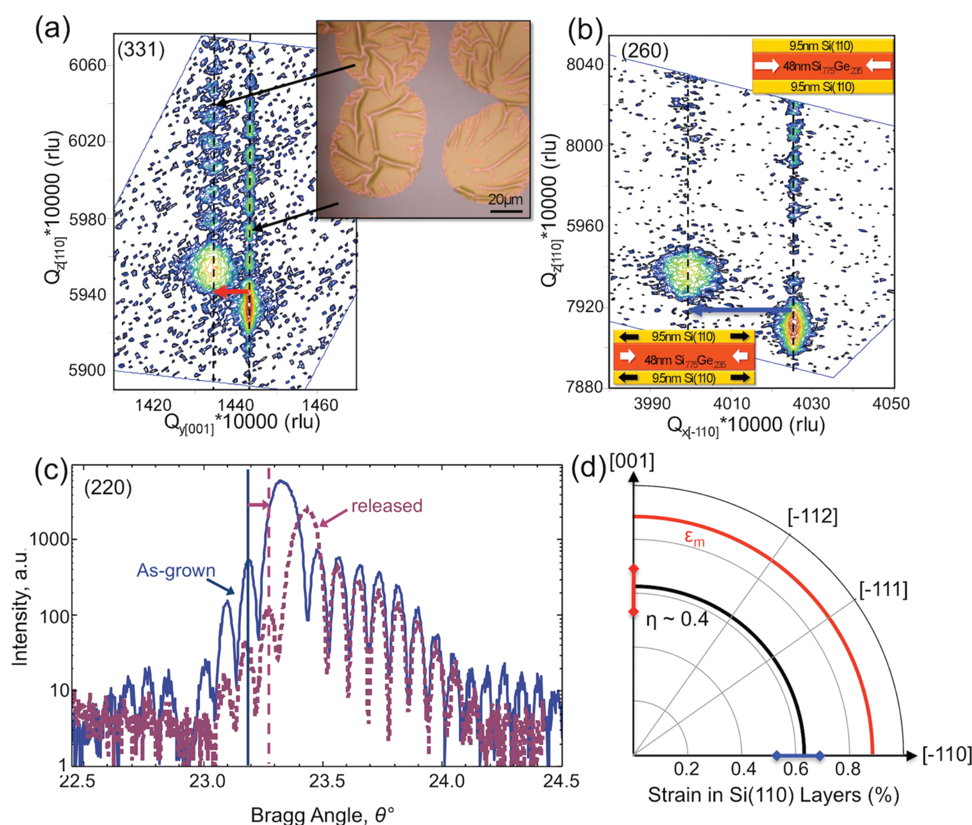


**Figure 6. Off-axis reciprocal-space maps (RSMs) around the (a) (331) and (b) (260) reflections for the partially released trilayer Si(110) NM. An optical micrograph of the partially released trilayer Si(110) NM is shown in the inset of (a). At the center of each of the pink circular regions, there is a 5 $\mu$m hole to allow the etchant access to the underlying $SiO_2$ layer: these regions are free to strain share (expansion causes wrinkles in the NM) as the supporting $SiO_2$ has been removed. A schematic diagram of the heterostructure is shown in the inset of (b) [top is as-grown state, bottom is released state]. The RSMs indicate that the alloy layer lattice constant becomes larger in-plane (decrease in reciprocal lattice units) and becomes smaller out-of-plane (increase in reciprocal lattice units). The amount of in-plane strain in each in-plane direction, {[001] (red arrow), [$\bar{1}$10] (blue arrow)} is the change in in-plane lattice constant over the initial in-plane lattice constant $\Delta a_{\|}/a_{\|}$ = 0.6 ± 0.1%. (c) (220) $\theta/2\theta$ XRD scan of the same trilayer before release (—) and after a full release (- - -). The uniform shift (0.08°) indicates elastic strain sharing and an out-of-plane strain relaxation, $\varepsilon_{\perp}$ = 0.32 ± 0.04%, which translates into an in-plane strain, $\varepsilon_{\|}$ = 0.64 ± 0.09%. The measurements closely agree with the expected strain transfer as calculated from eq 4 for this heterostructure (d).**

Figure 6a,b indicates that the Si and SiGe layers have the same in-plane lattice constant (the Si peak lies along a line with the same horizontal position as the SiGe), thus indicating proper strain sharing between the three layers. Equal strain in two dissimilar perpendicular in-plane directions means that with elastic strain sharing we obtain isotropic strain relaxation in the alloy layer upon release, implying that the in-plane biaxial strain in the Si is also isotropic.

*Acknowledgment.* The authors thank K.T. Turner and H.J. Kim-Lee for helpful discussions. This research was supported by DOE, Grant No. DE-FG02-03ER46028. Facilities support by NSF, MRSEC program, is acknowledged. D.M.P. acknowledges support from the National Defense Science and Engineering Graduate (NDSEG) Fellowship Program and NSF Graduate Research Fellowship Program. S.A.S. acknowledges fellowship support from the New Zealand Foundation for Research Science and Technology (FRST). SOI(110) materials were provided by Soitec, Inc.

## REFERENCES AND NOTES

1. Sun, Y.; Thompson, S. E.; Nishida, T. Physics of Strain Effects in Semiconductors and Metal-Oxide-Semiconductor Field-Effect Transistors. *J. Appl. Phys.* **2007**, *101*, 104503.
2. Fischetti, M. V.; Ren, Z.; Solomon, P. M.; Yang, M.; Rim, K. Six-Band K•P Calculation of the Hole Mobility in Silicon Inversion Layers: Dependence on Surface Orientation, Strain, and Silicon Thickness. *J. Appl. Phys.* **2005**, *94*, 1079–1095.
3. Grundmann, M.; Stier, O; Bimberg, D. InAs/GaAs Pyramidal Quantum Dots: Strain Distribution, Optical Phonons, and Electronic Structure. *Phys. Rev. B* **1995**, *52*, 11969–11981.
4. Schäffler, F. High-Mobility Si and Ge Structures. *Semicond. Sci. Technol.* **1997**, *12*, 1515–1549.
5. Sun, Y.; Thompson, S. E.; Nishida, T. *Strain Effect in Semiconductors: Theory and Device Applications*; Springer: New York, 2010.
6. Nieto, J. M.; Comas, F. Polar Optical Phonons in a Semiconductor Quantum-Well: The Complete Matching Problem. *Physica B* **2007**, *388*, 153–158.
7. Liu, F.; Wu, F.; Lagally, M. G. Effect of Strain on Structure and Morphology of Ultrathin Ge on Si(001). *Chem. Rev.* **1997**, *97*, 1045–1061.
8. Cao, J.; Wu, J. Strain Effects in Low-Dimensional Transition Metal Oxides. *Mater. Sci. Eng. R* **2011**, *71*, 35–52 and references therein.
9. Thornton, J. A.; Hoffman, D. W. The Influence of Discharge Current on the Intrinsic Stress in Mo Films Deposited Using Cylindrical and Planar Magnetron Sputtering Sources. *J. Vac. Sci. Technol., A* **1985**, *3*, 576–579.
10. Tamulevičius, S. Stress and Strain in Vacuum Deposited Thin Films. *Vacuum* **1998**, *51*, 127–139.
11. Matthews, J. W.; Blakeslee, A. E. Defects in Epitaxial Multilayers: I. Misfit Dislocations. *J. Cryst. Growth* **1974**, *27*, 118–125.
12. Chu, M.-W.; Szafraniak, I.; Scholz, R.; Harnagea, C.; Hesse, D.; Alexe, M.; Gösele, U. Impact of Misfit Dislocations on the Polarization Instability of Epitaxial Nanostructured Ferroelectric Perovskites. *Nat. Mater.* **2004**, *3*, 87.

13. Monroe, D.; Xie, Y. H.; Fitzgerald, E. A.; Silverman, P. J.; Watson, G. P. Comparison of Mobility-Limiting Mechanism in High-Mobility $Si_{1-x}Ge_x$ Heterostructures. *J. Vac. Sci. Technol., B* **1993**, *11*, 1731–1737.
14. Borak, A.; Tsujino, S.; Falub, C.; Scheinert, M.; Diehl, L.; Müller, E.; Sigg, H.; Grützmacher, D.; Kermarrec, O.; Bensahel, D.; *et al.* Recent Results on the Road to a Si/SiGe Quantum Cascade Laser. *Mater. Res. Soc. Symp. Proc.* **2005**, *832*, F4.2.1.
15. Roberts, M. M.; Klein, L. J.; Savage, D. E.; Slinker, K. A.; Friesen, M.; Celler, G.; Eriksson, M. A.; Lagally, M. G. Elastically Relaxed Free-Standing Strained-Silicon Nanomembranes. *Nat. Mater.* **2006**, *5*, 388–393.
16. Scott, S. A.; Lagally, M. G. Elastically Strain-Sharing Nanomembranes: Flexible and Transferable Strained Silicon and Silicon−Germanium Alloys. *J. Phys. D: Appl. Phys.* **2007**, *40*, R75–R92.
17. Yuan, H.-C.; Kelly, M. M.; Savage, D. E.; Lagally, M. G.; Celler, G. K.; Ma, Z. Thermally Processed High-Mobility MOS Thin-Film Transistors on Transferable Single-Crystal Elastically Strain-Sharing Si/SiGe/Si Nanomembranes. *IEEE Trans. Electron Devices* **2008**, *55*, 810–815.
18. Sun, Y.; Menard, E.; Rogers, J. A.; Kim, H.-S.; Kim, S.; Chen, G.; Adesida, I.; Dettmer, R.; Cortez, R.; Tewksbury, A. Gigahertz Operation in Flexible Transistors on Plastic Substrates. *Appl. Phys. Lett.* **2006**, *88*, 183509.
19. Huang, M. H.; Ritz, C. S.; Novakovic, B.; Yu, D.; Zhang, Y.; Flack, F.; Savage, D. E.; Evans, P. G.; Knezevic, I.; Liu, F.; *et al.* Mechano-Electronic Superlattices in Silicon Nanoribbons. *ACS Nano* **2009**, *3*, 721–727.
20. Deneke, C.; Songmuang, R.; Jin-Phillipp, N. Y.; Schmidt, O. G. The Structure of Hybrid Radial Superlattices. *J. Phys. D: Appl. Phys.* **2009**, *42*, 103001.
21. Liu, Z.; Wu, J.; Duan, W.; Lagally, M. G.; Liu, F. Electronic Phase Diagram of Single-Element Silicon "Strain" Superlattice. *Phys. Rev. Lett.* **2010**, *105*, 016802.
22. Owen, D. L.; Lackner, D.; Pitts, O. J.; Watkins, S. P.; Mooney, P. M. In-Place Bonding of GaAs/InGaAs/GaAs Heterostructures to GaAs(001). *Semicond. Sci. Technol.* **2009**, *24*, 035011.
23. Seo, S. W.; Lee, K. K.; Kang, S.; Huang, S.; Doolittle, W. A.; Jokerest, N. M.; Brown, A. S. GaN Metal−Semiconductor−Metal Photodetectors Grown on Lithium Gallate Substrates by Molecular-Beam Epitaxy. *Appl. Phys. Lett.* **2001**, *79*, 1372–1375.
24. Albu, S. P.; Ghicov, A.; Macak, J. M.; Hahn, R.; Schmuki, P. Self-Organized, Free-Standing $TiO_2$ Nanotube Membranes for Flow-Through Photocatalytic Applications. *Nano Lett.* **2010**, *7*, 221901.
25. Chen, J.-J.; Jang, S.; Ren, J. F.; Li, Y.; Kim, H.-S.; Norton, D. P.; Pearton, S. J.; Osinsky, A.; Chu, S. N. G.; Weaver, J. F. Selective and Nonselective Wet Etching of $Zn_{0.9}Mg_{0.1}$/ZnO. *J. Electron. Mater.* **2006**, *35*, 516–519.
26. Yin, W.-J.; Chen, S; Yang, J.-H.; Gong, X.-G.; Yan, Y.; Wei, S.-H. Effective Bandgap Narrowing of Anatase $TiO_2$ by Strain along a Soft Direction. *Appl. Phys. Lett.* **2010**, *96*, 221901.
27. Nam, Y. S.; Lee, S. W.; Baek, K. S.; Chang, S. K.; Song, J.-H.; Song, J.-H.; Han, S. K.; Yao, T. Anisotropic Optical Properties of Free and Bound Excitons in Highly Strained *A*-Plane ZnO Investigated with Polarized Photoreflectance and Photoluminescence Spectroscopy. *Appl. Phys. Lett.* **2008**, *92*, 201907.
28. Shan, W.; Fischer, A. J.; Song, J. J.; Bulman, G. E.; Kong, G. E.; Leonard, M. T.; Perry, W. G.; Bremser, M. D.; Davis, R. F. Optical Studies of GaN and GaN/AlGaN Heterostructures on SiC Substrates. *Appl. Phys. Lett.* **1996**, *69*, 740–743.
29. Huang, M. H.; Boone, C.; Roberts, M.; Savage, D. E.; Lagally, M. G.; Shaji, N.; Qin, H.; Blick, R.; Naim, J. A.; Liu, F. Nanomechanical Architecture of Strained Bilayer Thin Films: From Design Principles to Experimental Fabrication. *Adv. Mater.* **2005**, *17*, 2860–2864.
30. Song, J.; Jiang, H.; Huang, Y; Rogers, J. A. Mechanics of Stretchable Inorganic Electronic Materials. *J. Vac. Sci. Technol., A* **2009**, *27*, 1107–1125.
31. Freund, L. B.; Suresh, S. *Thin Film Materials: Stress, Defect Formation, and Surface Evolution*; Cambridge University Press: Cambridge, MA, 2003.
32. Kiefer, A. M.; Paskiewicz, D. M.; Clausen, A. M.; Buchwald, W. R.; Soref, R. A.; Lagally, M. G. Si/Ge Junctions Formed by Nanomembrane Bonding. *ACS Nano* **2011**, *5*, 1179–1189.
33. Bai, G.; Ma, W. Phenomenological Analysis of Phase Transistions in Epitaxial Perovskite Ferroelectric Thin Films. *Physica B* **2010**, *405*, 1901–1907.
34. Wortman, J. J.; Evans, R. A. Young's Modulus, Shear Modulus, and Poisson's Ratio in Silicon and Germanium. *J. Appl. Phys.* **1965**, *36*, 153–156.
35. Opotowsky, A. C.; Scott, S. A.; Ritz, C. S.; Savage, D. E.; Celler, G. K.; Lagally, M. G. Structure of Elastically Strain-Sharing Silicon(110) Nanomembranes. *New J. Phys.* **2007**, *7*, 270.
36. Paskiewicz, D. M.; Scott, S. A.; Savage, D. E.; Lagally, M. G. Elastically Strain-Sharing Si(110) Nanomembranes. *ECS Trans.* **2010**, *33*, 813–821.
37. Arimoto, K.; Yamamamka, J.; Nakagawa, K.; Sawano, K.; Shiraki, Y.; Usami, N.; Nakajima, K. Growth Temperature Dependence of Lattice Structures of SiGe/Graded Buffer Structures Grown on Si(110) Substrates by Gas-Source MBE. *J. Cryst. Growth* **2007**, *301*, 343–348.
38. Destefanis, V.; Rouchon, D.; Hartmann, J. M.; Papon, A. M.; Baud, L.; Crisci, A.; Mermoux, M. Structural Properties of Tensily Strained Si Layers Grown on SiGe (100), (110), and (111) Virtual Substrates. *J. Appl. Phys.* **2009**, *106*, 043508.
39. Zhang, X.; Pashley, D. W. Comparison of the Strain Relief Behavior of $In_xGa_{1-x}As$ Alloy on GaAs (001) and (110) Substrates. *J. Mater. Sci.: Mater. Electron.* **1996**, *7*, 361–367.
40. Koch, R. The Intrinsic Stress of Polycrystalline and Epitaxial Thin Metal Films. *J. Phys.: Condens. Matter* **1994**, *6*, 9519–9550.
41. Liu, B. Z.; Nogmai, J. A Scanning Tunneling Microscopy Study of Dysprosium Silicide Nanowire Growth on Si(001). *J. Appl. Phys.* **2003**, *93*, 593–599.
42. Mack, S.; Meitl, M. A.; Baca, J.; Zhu, Z.-T.; Rogers, J. A. Mechanically Flexible Thin-Film Transistors that Use Ultrathin Ribbons of Silicon Derived from Bulk Wafers. *Appl. Phys. Lett.* **2006**, *88*, 213101.
43. Liu, B. Z.; Nogmai, J. Growth of Parallel Rare-Earth Silicide Nanowire Arrays on Vicinal Si(001). *Nanotechnology* **2003**, *14*, 873–877.
44. Jacobsen, R. S.; Andersen, K. N.; Borel, P. I.; Fage-Pedersen, J.; Frandsen, L. H.; Hansen, O.; Kristensen, M.; Lavrinenko, A. V.; Moulin, G.; Ou, H.; *et al.* Strained Silicon as a New Electro-optic Material. *Nature* **2006**, *441*, 199–202.
45. Zhang, F. H.; Huang, Z.; Gao, G. Y.; Chen, P. F.; Wang, L. F.; Tan, X. L.; Wu, W. B. Anisotropic-Strain-Induced Antiferromagnetic-Insulating State with Strong Phase Instability in Epitaxial $(La_{0.8}Pr_{0.2})_{0.67}Ca_{0.33}MnO_3$ Films. *Appl. Phys. Lett.* **2010**, *96*, 062507.
46. Houghton, D. C. Strain Relaxation Kinetics in $Si_{1-x}Ge_x$/Si Heterostructures. *J. Appl. Phys.* **1991**, *70*, 2136–2151.
47. Eriksson, M. A.; Friesen, M.; Coppersmith, S. N.; Joynt, R.; Klein, L. J.; Slinker, K.; Tahan, C.; Mooney, P. M.; Chu, J. O.; Koester, S. J. Spin-Based Quantum Dot Quantum Computing in Silicon. *Quantum Inf. Process.* **2004**, *3*, 133–146.
48. Jampana, B. R.; Faleev, N. N.; Ferguson, I. T.; Opila, R. L.; Honsberg, C. B. Utilizing Polarization Induced Band Bending for InGaN Solar Cell Design. *Mater. Res. Soc. Symp. Proc.* **2009**, *1167*, 1167-O7-04.
49. Mooney, P. M. Strain Relaxation and Dislocations in SiGe/Si Structures. *Mater. Sci. Eng.* **1996**, *R17*, 105–146.
50. Dubourdieu, C.; Gélard, I.; Salicio, O.; Saint-Girons, G.; Vilquin, B.; Hollinger, G. Oxide Heterostructures for Nanoelectronics. *Int. J. Nanotechnol.* **2010**, *7*, 320–347.
51. Ting, T. C. T. *Anisotropic Elasticity: Theory and Applications*; Oxford University Press: New York, 1996.
52. Floro, J. A.; Chason, E.; Lee, S. R.; Petersen, G. A. Biaxial Moduli of Coherent $Si_{1-x}Ge_x$ Films on Si(001). *Appl. Phys. Lett.* **1997**, *71*, 1694–1696.
53. Mathiondakis, C.; Kelires, P. C. Softening of Elastic Moduli of Amorphous Semiconductors. *J. Non-Cryst. Solids* **2000**, *266−269*, 161–165.